High-spatiotemporal-quality petawatt-class laser system

Hiromitsu Kiriyama,[1,*] Mori Michiaki,[1] Yoshiki Nakai,[1] Takuya Shimomura,[1] Hajime Sasao,[1] Momoko Tanaka,[1] Yoshihiro Ochi,[1] Manabu Tanoue,[1] Hajime Okada,[1] Shuji Kondo,[1] Shuhei Kanazawa,[1] Akito Sagisaka,[1] Izuru Daito,[1] Daisuke Wakai,[1] Fumitaka Sasao,[1] Masayuki Suzuki,[1] Hideyuki Kotakai,[1] Kiminori Kondo,[1] Akira Sugiyama,[1] Sergei Bulanov,[1] Paul R. Bolton,[1] Hiroyuki Daido,[1] Shunichi Kawanishi,[1] John L. Collier,[2] Cristina Hernandez-Gomez,[2] Chris J. Hooker,[2] Klaus Ertel,[2] Toyoaki Kimura,[3] and Toshiki Tajima[1,4]

[1]Advanced Photon Research Center and Photo-Medical Research Center, Japan Atomic Energy Agency, 8-1-7 Umemidai, Kizugawa-city, Kyoto, 619-0215, Japan

[2]Central Laser Facility, Science and Technology Facilities Council Rutherford Appleton Laboratory, Chilton, Didcot OX11 0QX, United Kingdom

[3]Japan Synchrotron Research Institute, 1-1-1 Kouto, Sayo-cho, Sayo-gun, Hyogo 679-5198, Japan

[4]Sekiton Physik, Ludwing-Maximilians-Universität, Am Coulombwall 1, D-85748 Garching, Germany

*Corresponding author: kiriyama.hiromitsu@jaea.go.jp

Received 3 December 2009; revised 15 March 2010; accepted 15 March 2010; posted 17 March 2010 (Doc. ID 120918); published 5 April 2010

We have developed a femtosecond high-intensity laser system that combines both Ti:sapphire chirped-pulse amplification (CPA) and optical parametric CPA (OPCPA) techniques and produces more than 30 J broadband output energy, indicating the potential for achieving peak powers in excess of 500 TW. With a cleaned high-energy seeded OPCPA preamplifier as a front end in the system, for the compressed pulse without pumping the final amplifier, we found that the temporal contrast in this system exceeds 10^{10} on the subnanosecond time scales, and is near 10^{12} on the nanosecond time scale prior to the peak of the main femtosecond pulse. Using diffractive optical elements for beam homogenization of a 100 J level high-energy Nd:glass green pump laser in a Ti:sapphire final amplifier, we have successfully generated broadband high-energy output with a near-perfect top-hat-like intensity distribution.

OCIS codes: 320.7090, 190.4970, 170.7160, 140.3280, 230.4480.

1. Introduction

The invention of chirped-pulse amplification (CPA) [1] together with titanium-doped sapphire (Ti: sapphire) media have enabled generation of ultrashort laser pulses with high intensity, accessing opportunities for experimental study of the behavior of matter in ultrahigh electromagnetic fields in small-scale laboratories [2,3]. Recently much effort in CPA laser development has been expended toward achieving high intensities, such as the 100 TW or even petawatt power level [4–9]. Consequently, high-intensity laser–matter interaction studies can now be done with focused peak intensities in the 10^{20} W/cm^2 range or more [7,10]. This progress in high-field

0003-6935/10/112105-11$15.00/0

science gives rise to the birth of new applications and breakthroughs, which include relativistic particle acceleration [11–14], bright x-ray source generation [15–17], and nuclear activation [18].

To reach these intensities, great effort has been directed to increasing the pulse energy and reducing the pulse duration. For many experiments, increased peak intensities require a commensurate improvement in temporal contrast. Here, the temporal contrast (referred to henceforth as, simply, contrast) is taken to be the ratio of the peak intensity of the main pulse to the intensity of the amplified spontaneous emission (ASE) background and has values much greater than one. The temporal contrast is a critical characteristic of femtosecond high-intensity laser pulses for many experiments where it is important to avoid any modification of the target, such as preplasma formation, before arrival of the main femtosecond laser pulse [19,20]. For example, with intensities greater than 10^{20} W/cm^2 and contrast in the range of 10^6–10^8, the prepulse intensity level (and duration) is above threshold for pre-plasma formation on a solid target. In this low-contrast case, the ASE alters the physical condition of the target for the main intense pulse. To avoid preplasma formation before the main femtosecond pulse of such high-intensity arrives, it is essential to increase the contrast level to 10^{10} or more. The use of high-contrast pulses for interaction of high-intensity lasers with solid targets is of primary importance for a number of experiments. Specifically, experimental data and particle-in-cell simulations of laser acceleration of ions suggest the maximum proton energy increases significantly as the target thickness is reduced for sufficiently high laser intensity and contrast [11,12,20]. Because contrast is crucial for accessing high-field physics in desired targets, it has become a major issue, and is today under serious investigation throughout the world. Some techniques for improving the contrast of high-intensity lasers, such as the use of saturable absorbers [21,22], nonlinear Sagnac interferometers [23], double CPA laser system architecture [24], cross-polarized wave (XPW) generation in nonlinear crystals [25,26], and self-induced plasma shuttering (also called "plasma mirror") [27,28], have been proposed and tested. More recently, the XPW has been investigated and s temporal contrast of over 10^{10} has been reported at multiterawatt power levels [29]. However, this has not yet been implemented in petawatt-class laser systems. In addition, the efficiency of this technique is limited to the range of 10%–20%, although input intensity can be at the TW/cm^2 level [30,31]. The plasma mirror is a simpler, more effective and more robust technique that can be applied at the full compressed pulse energy focused to high fluence levels for which there are consequently no additional downstream contributions to ASE. Therefore, the plasma mirror is used in many laboratories, and significant improvement in the contrast, to levels much greater than 10^{10}, have been reported [28]. However, the single-stage efficiency is typically no more than $\sim$70% [27], and it is challenge to implement this technique at high repetition rates because each targeted area is used once for each laser shot. Optical parametric CPA (OPCPA) [31,32] is becoming increasingly popular as a front-end preamplifier system that can significantly improve contrast, but has been evaluated only for the front end of a petawatt-class Nd:glass laser system for fusion research [33–36] upstream of an amplifier chain and where the pulse energy is much lower. The use of an OPCPA preamplifier in a petawatt-class high-intensity Ti:sapphire laser has not been studied, to our knowledge.

Homogeneous flat-top circular profiles with steep edges are needed to pump a large-aperture Ti:sapphire crystal, to enable high beam quality CPA systems at the petawatt power level. In petawatt-class systems, the flat-top transverse beam profile is required for both amplification efficiency and to guarantee operation below the damage threshold on large-aperture Ti:sapphire crystals and large gratings, which are typically very expensive optical components in the system. Frequency-doubled large-aperture high-energy Nd:glass green lasers are widely used to pump petawatt-class laser systems [4–6,8,9]. The flat-top beam profile is required from the pump lasers to maintain acceptable beam quality, reliable damage-free operation, and to increase amplification efficiency. However, the direct output beam of the Nd:glass laser system typically exhibits a poor (unacceptable) spatial beam profile, which can lead to local hot spots (high intensity). These hot spots can induce intensity modulations and enhance parasitic transverse lasing. It is necessary to control the green pump profile to achieve a mandatory flat-top distribution. Some methods for maintaining the flat-top profile of Nd:glass green pump lasers have been investigated, such as image relaying (with spatial filtering in some cases) [4,5,8] and the use of a microlens array [37]. The shaping the glass pump beam profile with a microlens array homogenizing system has been demonstrated [37]. The working principle of this technique is to divide the incident beam into many subapertures, which are all expanded onto the same area in the so-called target plane that lies inside the laser crystal. The resulting profile in the target plane, however, can exhibit the Talbot effect, which might result in low amplification efficiency due to low beam overlap efficiency. The utilization of diffractive optical elements (DOE) has been proposed for profile homogenization. However, to date, there have been only a limited number of reports on beam homogenization of high-energy lasers using a DOE [38].

The development of energetic, intense laser systems with adequately high temporal contrast and high spatial quality remains an important challenge. The development of such laser sources will bring us closer to the realization of compact energetic proton, electron, or x-ray sources that can potentially revolutionize medical and industrial science and technology.

In this paper, we describe a temporally and spatially high-quality petawatt laser system (which we have named J-KAREN). The system utilizes a cleaned ("cleaned" refers to ASE pedestal suppression) high-energy seeded low-gain OPCPA preamplifier in a double CPA architecture with extremely high temporal contrast. DOEs are used for beam homogenization of a 100 J class high-energy green pump laser for achieving a highly spatially flat-topped amplified beam. We have demonstrated over 30 J of uncompressed broadband output energy from this system, indicating potential for reaching peak power above 500 TW with a pulse energy of 20 J and compressed duration of less than 40 fs, and with a temporal contrast exceeding 10^{10}. Because state-of-the-art petawatt-class CPA laser facilities use Ti:sapphire amplifiers, temporal contrast is in the approximate range of 10^{6}–10^{8}. Specifically, the use of double CPA with an OPCPA preamplifier and a Ti:sapphire main amplifier leads to extremely high temporal contrast in the petawatt-class power range. An efficient beam homogenization scheme using DOEs produces a broadband amplified flat-topped output with a 70% filling factor. To the best of our knowledge, this is the first petawatt-class hybrid laser system that combines both Ti:sapphire CPA and OPCPA techniques, and the first to evaluate the filling factor values for the spatial profile for both pump and amplified broadband beams with DOEs. The performance of this high-intensity laser system will enable many high-field applications.

2. Design and Performance of J-KAREN Laser System

A schematic of the J-KAREN laser system is shown in Fig. 1. The system consists of two successive CPA stages linked by a saturable absorber, which acts as a nonlinear temporal filter. The first CPA stage consists of an oscillator, a stretcher, a nine-pass amplifier and a compressor. The second CPA stage consists of a stretcher (using 1480 grooves/mm gratings), a two-stage OPCPA preamplifier, a four-pass Ti:sapphire preamplifier, a four-pass cryogenically cooled Ti:sapphire power amplifier, a three-pass Ti:sapphire final booster amplifier and a compressor that consists of four 1480 grooves/mm gratings.

A. Front-End System

In the first CPA stage, we use a compact commercial Ti:sapphire CPA laser system (Femtolasers, Femtopower Compact Pro). This system produces submillijoule, sub-30 fs pulses at a repetition rate of 1 kHz. Part of the ASE pedestal on these femtosecond pulses from the first CPA system is initially removed by transmission through a saturable absorber. We avoid thermally induced damage to the saturable absorber by operating a Pockels cell at a 10 Hz repetition rate in the nine-pass amplifier, which then transmits pulses to the absorber and on to the second CPA stage of J-KAREN at only 10 Hz. The remaining pulses at 990 Hz will be directed to other experimental areas. The pulses are transmitted through the saturable absorber with 20% efficiency and then these cleaned microjoule pulses are sent to the second CPA stage. It is important to note that the main laser pulses must be compressed to femtosecond durations at the input of the saturable absorber in order to remove the unwanted ASE portion (hence the need for a double-CPA architecture).

The challenge is to generate the high-energy, cleaned femtosecond laser pulses for the second CPA stage. By injecting high-energy cleaned seed pulses into the second CPA stage, the amplification ratio (gain) in the second is kept low and, therefore, the final ASE level can be suppressed.

B. OPCPA Preamplifier

In the second CPA stage, the OPCPA preamplifier replaces the more conventional regenerative amplifier in order to maintain the high contrast and broad spectral bandwidth. As input to the OPCPA, cleaner seed pulses of energy 2.5 μJ are temporally restretched to ~1 ns duration (FWHM) by an all-reflective Öffner stretcher [39]. The stretcher is composed of gratings with a groove density of 1480 grooves/mm, a 1000 mm radius of curvature concave mirror (320 mm

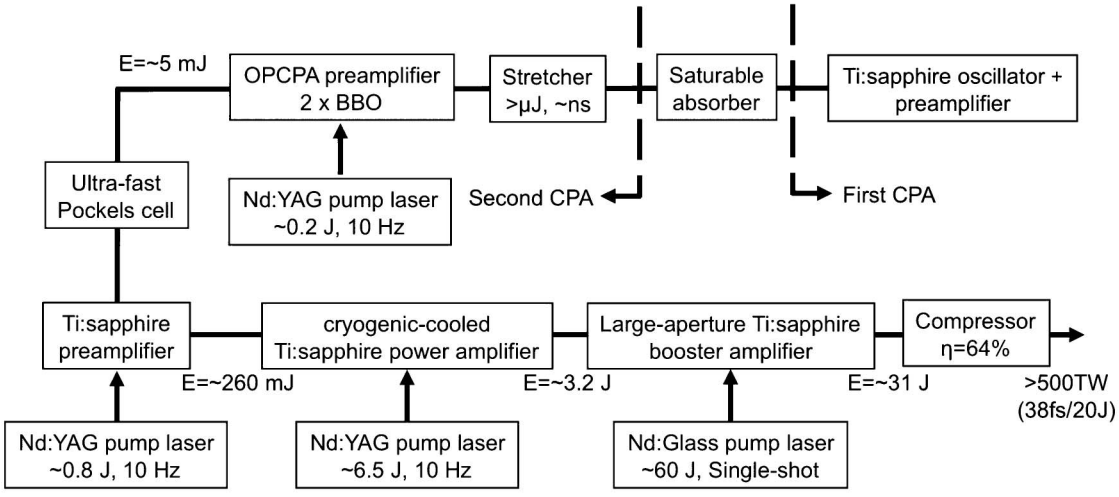

Fig. 1. Optical layout of the J-KAREN laser.

diameter), a –500 mm radius of curvature convex mirror (160 mm long, 15 mm high), and a roof mirror. A Faraday isolator and the Pockels cell with a pair of polarizers provide needed optical isolation between the oscillator and the Öffner stretcher. Parametric fluorescence is known to degrade contrast in the high-gain regime where seed energies are low (of the order of nanojoules) and pump intensities are high. Therefore, contrast improvement can be mitigated with higher seed energy levels (2.5 μJ) and a lower OPCPA gain requirement [40–42]. Our OPCPA preamplifier consists of two β-barium borate (BBO) crystals. A BBO crystal is chosen as the nonlinear crystal because of its high effective nonlinear coefficient. The crystals have a oss ection of 7 mm × 7 mm and their lengths are 19.5 mm. Both antireflection-coated (AR-coated) crystals are cut at 23.8° to maximize the gain bandwidth and to facilitate type I noncollinear angular phase matching with an external angle between the seed and the pump of 3.9°. Each crystal is mounted on a precision rotation stage to optimize the angle between the input beams and the crystal. A common pump pulse is used for the OPCPA to reduce the system size and complexity. Each crystal has a 2° wedged output face to suppress intracavity oscillation [22,43].

A commercial frequency-doubled, *Q*-switched single-longitudinal-mode Nd:YAG laser operating at 532 nm (Spectra-Physics, Quanta-Ray Pro-230-10) pumps the OPCPA stages at 10 Hz with pulse energy over 300 mJ within a 9.7 ns (FWHM) duration. The output temporal profile is smooth and near-Gaussian and the spatial profile almost a flattop. Pump pulses are relayed to a plane between the two BBO crystals with a vacuum image telescope that precisely matches the pump beam diameter to that of the seed (~4.3 mm at the $1/e^2$ intensity points).

OPCPA gain is measured with a photodiode and a calibrated neutral density filter set. With an energy of 2.5 μJ, the input seed intensity is near 17 kW/cm^2. Most OPCPA systems operate with very high gain, of the order of 10^7–10^{11} [43–47]. However, our OPCPA provides a maximum gain of only ~1.8×10^3 with a pump energy of 208 mJ (corresponding to a pump intensity of 150 MW/cm^2) and amplifies the seed pulses to ~4.5 mJ. Parametric fluorescence can deteriorate the temporal pulse contrast when using the low seed energy in combination with the high pump intensities that are typical. Temporal pulse contrast can, therefore, be improved by operating the OPCPA in a higher seed energy, low-gain mode. Pump and seed pulses are synchronized in time by a Thales Laser ISEO unit, with a characteristic timing jitter of less than ±0.5 ns in our system. Automatic beam alignment systems for both seed and pump beams are used to implement beam adjustment to improve long-term stability. We obtain a measured shot-to-shot energy stability over 10 min of ±5% in our OPCPA system.

Using a saturable absorber is a simple way to remove the ASE, but it can also result in spectral narrowing in CPA systems. Within the OPCPA, altering the phase-match setting makes it possible to tune the central wavelength of the amplified pulse and, therefore, spectral shaping of the amplified pulse in a given spectral range is possible by cascading two BBO crystals working under slightly different phase-match settings. Another significant advantage of the OPCPA system [43,48] is that spectral control can also be achieved by varying the noncollinear pump-signal angle and the amplification pulse timing. In our system, the spectral bandwidth of the first CPA stage output is 42 nm (FWHM), which is reduced to 39 nm (FWHM) after passing through the saturable absorber. However, we obtain broader bandwidth of 53 nm (FWHM) by spectral shaping in the OPCPA preamplifier. The OPCPA output spectrum can also be optimized to better match the gain characteristics of the subsequent amplifiers.

C. Cryogenically Cooled Ti:Sapphire Power Amplifier

The nanosecond ASE pedestal on the OPCPA output pulse is eliminated with an ultrafast Pockels cell, which has a rise time of less than 150 ps. Following this "nanosecond" cleaning of the OPCPA output, a conventional four-pass Ti:sapphire preamplifier further amplifies the pulse energy. The preamplifier consists of a 20 mm diameter Ti:sapphire crystal with AR-coated faces and is pumped by a commercial frequency-doubled, *Q*-switched Nd:YAG laser (Continuum, Powerlite 9010) that delivers ~800 mJ (532 nm) pulse energy at 10 Hz. The pump beam is split into two beams that are relay imaged to opposite faces of the Ti:sapphire crystal. Image relaying is used throughout the optical train to minimize the diffractive effects, maintain beam uniformity, and to optimize coupling efficiency between the pump and the signal beams. Preamplification to a maximum output energy above 260 mJ is obtained with a ~700 mJ pump energy.

The pump laser also heats the Ti:sapphire crystal. Originating mainly from the difference between the pump and the amplified beam photon energies (quantum defect), heating generates a spatial refractive index gradient in the crystal, which is a source of unwanted thermal lensing of the amplified beam. Thermal lensing in Ti:sapphire gain media can be major problem if unaddressed in preamplifier design. So, in this Ti:sapphire preamplifier, the appropriate beam divergence is introduced (by adjusting the lenses separation in the upstream Galilean beam expander at the OPCPA exit), which matches the thermal focusing power of the Ti:sapphire preamplifier to counteract the thermal lens effect in the crystal. The input seed laser beam diameter is larger than the pump beam diameter. However, thermal focusing reduces the seed beam diameter to a collimated ~6 mm after four-pass amplification. At the Ti:sapphire preamplifier exit, the beam is subsequently up-collimated to an ~18 mm diameter and introduced into the four-pass cryogenically cooled Ti:sapphire power amplifier, which uses a 40 mm diameter AR-coated Ti:sapphire crystal. The power

amplifier is pumped at 10 Hz by ~6.5 J of second harmonic energy delivered by six commercial frequency-doubled, *Q*-switched Nd:YAG lasers (Spectra-Physics, Quanta-Ray Pro-350). All pump lasers are also image relayed to maintain a uniform spatial profile and to prevent damage to optics that can be caused by diffractive effects. As with the preamplifier, high average pump power can induce strong thermal lensing. We implemented cryogenic cooling to increase thermal conductivity, while reducing both refractive index gradient and the thermomechanical stress. Cryogenic cooling results in thermal focal lengths near 4,000 m under the maximum pumping condition, rendering thermal lensing insignificant [10,49–51].

Figure 2 shows the measured dependence of output energy from power amplifier on total pump energy at a 10 Hz repetition rate. The data are obtained by increasing the pump energy while maintaining the Ti:sapphire crystal temperature at 100 K in the cryogenic chamber. A maximum output energy of over 3.2 J is achieved with an incident pump energy of ~6.5 J. The excellent power stability of less than ±2% is observed over a 1 h interval, which is well in excess of the amplifier thermalization time at the highest pump level. The whole system is highly stable for several hours. The amplified pulse spectrum from the Ti:sapphire amplifier is redshifted due to saturation. As a mitigating measure, the amplifier input spectrum is, therefore, blueshifted by tuning the phase-match setting of the BBO crystals in the OPCPA preamplifier. We obtain the spectral bandwidth of over 45 nm from the power amplifier.

D. Large-Aperture Ti:Sapphire Booster Amplifier

The pulse undergoes final amplification in the booster amplifier, which uses a large-aperture 80 mm diameter Ti:sapphire crystal that is pumped with a frequency-doubled large-aperture high-energy Nd:glass laser. Our pump laser has single-pass master oscillator power amplifier architecture, operated at a few shots per hour. In the pump system, a long-cavity *Q*-switched Nd:YAG master oscillator generates ~200 mJ pulses of ~28 ns duration (FWHM) at a 1064 nm wavelength, which matches the emission band of the Nd:silicate-glass rod amplifiers. The duration of the oscillator pulse should be as long as possible to enable high-output fluence operation without optical damage. The oscillator output is shaped with a soft aperture to a near flat-top intensity distribution and then preamplified to ~1 J by a 9 mm diameter Nd:YAG rod preamplifier. The pulse energy is further increased in a chain of 16, 25, 45, and 64 mm diameter Nd:glass rod amplifiers to ~180 J. At appropriate locations, spatial filters and optical isolators (a pair of Faraday isolators) are used to suppress reflections that can cause damage upstream along the laser chain. The 1064 nm output pulses are down collimated to an ~40 mm diameter and are subsequently frequency doubled to 532 nm with two 60 mm × 60 mm Type II KD_2PO_4 (DKDP) crystals (Cleveland Crystals, Inc.). To achieve high conversion efficiency, we have used a quadrature arrangement for second harmonic generation (SHG), in which two nonlinear crystals cut for type II interaction are placed in series but are oriented perpendicular to each other [52,53]. DKDP crystals are chosen because of the easy availability in large sizes. The input and output faces of the crystals are SolGel AR coated for both 532 and 1064 nm laser radiation. In the pump system, a maximum green pulse energy of 96 J is generated with an incident fundamental energy of 177 J at 504 MW/cm^2, corresponding to an SHG efficiency of 54%. Dichroic mirrors separate the green and unconverted fundamental laser beams. With a half-wave plate and a thin-film polarizer, we generate an energy-balanced pair of green pump pulses from the DKDP crystals to provide similar energies for pumping both sides of the Ti:sapphire crystal. The two pulses are delivered to the Ti:sapphire crystal using reflective optics, image relaying, and DOEs (SILIOS Technologies). The polarization plane for one side is suitably oriented with respect to the Ti:sapphire crystal using a half-wave plate. We have selected DOEs for beam homogenization because they could produce a circular top-hat profile with sharp edges and they were readily available in the required size [9,38]. The clear aperture of our AR-coated DOEs is 80 mm. Each DOE is divided into about 200 subcells, which are all expanded onto the same area at the target plane that lies in the Ti:sapphire crystal. The eight-level striped pattern corresponding to the engravings in the subcells in 1 mm thick fused silica material are specially calculated for our requested shape [54]. The diffraction efficiency of DOE is measured to be 82%. Because of some optical components, such as half-wave plates, dichroic mirrors, thin-film polarizers, reflective optics, and relaying optics [55], the measured transmittance

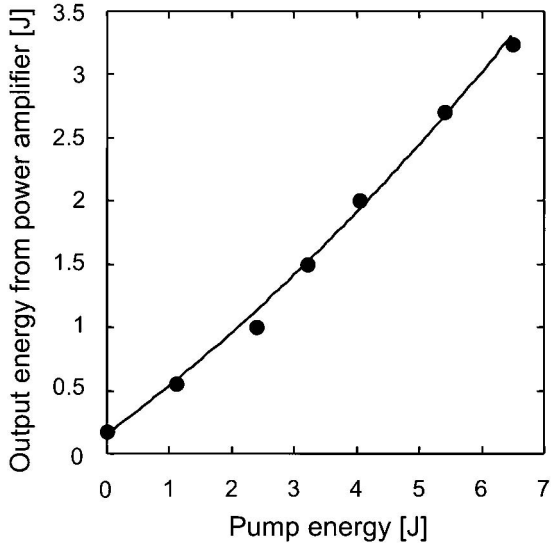

Fig. 2. Output energy from the cryogenically cooled power amplifier versus the incident pump energy.

efficiency from the second DKDP to Ti:sapphire crystal, including the DOE efficiency, is 67% in our case. The undiffracted and on-axis focused beams are dumped.

The pulses from power amplifier are up-collimated and enter the three-pass Ti:sapphire booster amplifier. The Ti:sapphire crystal is a commercially available disk (Crystal Systems, Inc.) that is 80 mm in diameter and 33 mm thick. The crystal is AR coated on two main surfaces, but not polished on the cylindrical outer surface. To suppress parasitic lasing that is associated with Fresnel reflection from the cylinder inner surface, we have employed a layer of index-matched thermoplastic polymer as absorption cladding, with a refractive index of 1.68 [4,56]. Parasitic lasing is further suppressed by matching (as closely as possible) the surrounding environment to the high refractive index (1.76) of Ti:sapphire (which clearly increases the loss of the parasitic cavities by decreasing Fresnel reflection). We are also testing other cladding material using refractive index-matched liquid with broadband-absorbing dye. The refractive index is 1.76 at 800 nm and we found that it bonds readily to the crystal's outer cylindrical surface. This reduces the reflection coefficient at normal incidence from 7% in the air down to 0.01%. The absorption coefficient at 532 nm for the crystal with the refractive index-matched liquid cladding, for example, is $0.78 \pm 0.25\,\mathrm{cm}^{-1}$. This cladding technique might overcome the technical difficulty of the long-term performance of the high-gain amplification and the cladding refreshment for large-aperture Ti:sapphire crystals. This technique would enable the J-KAREN amplifiers to increase output energy, repetition rate, and long-term stability in the future. The output energy of the booster amplifier with the thermoplastic polymer cladding is shown in Fig. 3. No energy saturation is observed within the investigated energy range. Thermal lensing in the booster amplifier is insignificant because of the low repetition rate. A maximum output energy of 31 J (uncompressed) is achieved with an incident pump energy of 56 J (an all optical conversion efficiency of greater than 50%).

E. Spatiotemporal Quality

The near-field spatial intensity distributions of the green pump beams from each DKDP crystal and the intensity distributions along the vertical and horizontal cross sections of these beams are also shown in Fig. 4. The near-field spatial intensity distributions are imaged by a CCD camera through a set of image-relay optics with high-energy (~100 J) green beams. As seen, the beams exhibit poor spatial qualities that are not suitable for directly pumping the Ti:sapphire amplifier. Most of the energy is concentrated in the outer edge area and, therefore, optical damage or parasitic oscillation could likely occur. Figure 5 shows the homogenized intensity distributions that are generated in the plane of the Ti:sapphire crystal for both pumping sides after passing through the DOEs. A maximum homogenized total green energy of 64 J is obtained at the Ti:sapphire crystal. From these figures, it is seen that near-perfect flat-topped intensity distributions are successfully generated and the DOE capability for beam homogenization is demonstrated. Because the use of beam homogenizers can prevent crystal damage and parasitic oscillation due to the spatial irregularities of pump beams, this should allow greater amplification by allowing pumping at higher fluence. Figure 6 shows the near-field spatial profiles of an over 30 J amplified broadband beam from the booster amplifier. The intensity distribution along the vertical and horizontal cross section of the beam is also shown. As seen, the beam profiles had near homogeneous flat-topped spatial intensity distributions. We have also evaluated the filling factor, which is defined as the ratio of peak intensity to average intensity of a spatial profile. A filling factor of 70% is obtained for over 30 J broadband output beam.

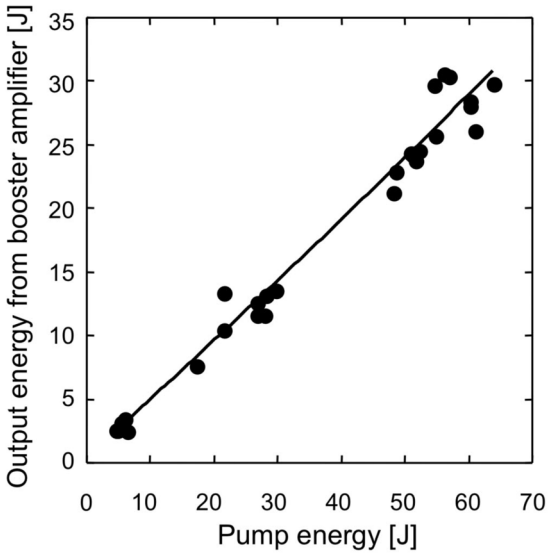

Fig. 3. Output energy from the booster amplifier versus the incident pump energy.

The pulse from the booster amplifier is also expanded to 120 mm through a spatial filter and then directed to the pulse compressor, which consists of four 1480 grooves/mm gratings. The measured

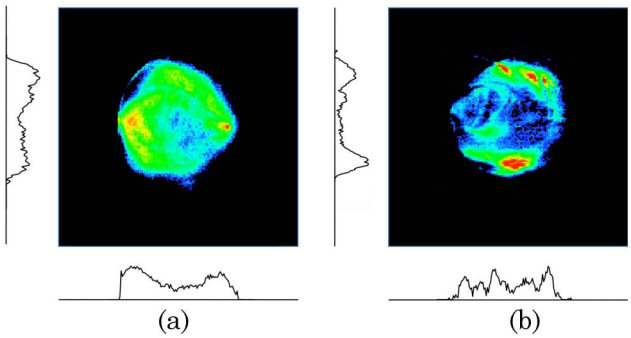

Fig. 4. (Color online) Spatial distributions of output intensity from each DKDP crystal: (a) first crystal and (b) second crystal.

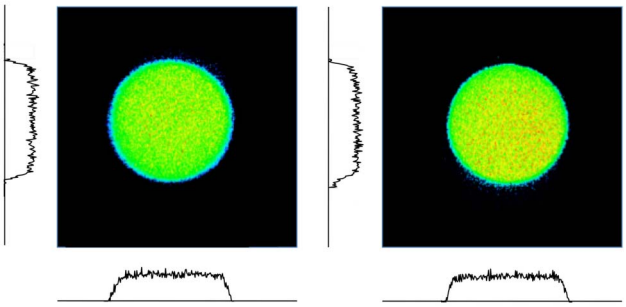

Fig. 5. (Color online) Spatial distributions of intensity of the homogenized pump beam at each Ti:sapphire crystal side.

throughput of the pulse compressor is 64%, which would correspond to compressed energy of 20 J with a 30 J uncompressed input. We measure the pulse duration without pumping the booster amplifier. The pulse duration is measured to be 38 fs with a fluctuation of less than ±5% using a frequency-resolved optical gating. An average pulse duration of 38 fs indicates the potential for peak power of greater than 500 TW.

We also measure the contrast without pumping the booster amplifier. The contrast for attenuated, amplified, compressed pulses is measured using the third-order cross correlator (Sequoia unit by Amplitude Technologies) in order to characterize the contrast on a subnanosecond time scale. A uncompressed high-energy beam of over 3 J is attenuated by a beam attenuation line to prevent the optical damage on the third-order cross correlator. The beam attenuation line consisted of a half-wave plate and two polarizers. This beam attenuation line exhibits a net variable extinction of greater than 10^2. These optics are placed in a collimated beam line after the power amplifier in order to maintain the same beam quality, such as beam divergence. The attenuated beam is then passed through the booster (final) amplifier, without pumping, and the compressor. To deliver the high-energy beam, we just rotated the half-wave plate. Because the high-energy beam and the attenuated beam follow the same path and undergo the same pumping condition, the actual contrast is unaltered with increased pulse energy. Figure 7 shows the temporal pulse trace with delays from 500 ps prior to the main femtosecond pulse to 150 ps past the main pulse. We average over ten shots to obtain each individual data point. The peaks around the main pulse are attributed to multiple reflections of the main pulse at the optical components in the down-collimation beam line and the third-order cross correlator. The post pulses act as prepulses for the third-order cross-correlation signal. The background level observed is 10^{-10} relative to the main pulse. Because of pulse broadening of the femtosecond main pulse by group velocity dispersion in optical components inside the present correlator, the measured contrast from Fig. 7 is actually better than that shown in the figure. Thus, we can conclude that the contrast is at least 10^{10} on subnanosecond time scales. At the −100 ps delay, contrast degradation may come from noise on the OPCPA pump pulse [57,58]. Further investigation is required to fully evaluate and confirm this contrast degradation mechanism. However, one can also see that 99% of the energy is contained in the main pulse from 0.25 ps prior to peak intensity to 0.25 ps past the peak intensity. The residual 1% of the energy is distributed over a 650 ps wide pedestal from 500 ps before the peak intensity to 150 ps after the peak intensity. We have used the numerical model based on the Frantz–Nodvik equation [59] and have calculated the gains of the booster amplifier at the maximum pumping conditions for the main pulse and the ASE. The

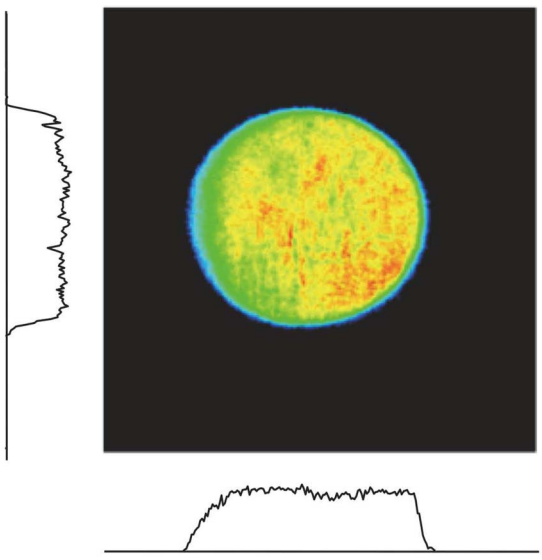

Fig. 6. (Color online) Spatial intensity distribution of the booster amplifier output.

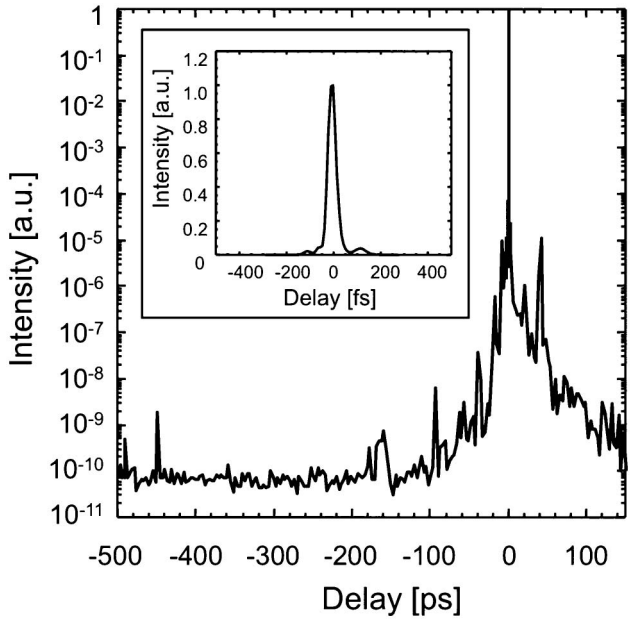

Fig. 7. Temporal contrast. Inset is the recompressed pulse.

calculated gain values for the main pulse and the ASE are 12 and 34, respectively. Taking account the calculated gain values, the measured contrast without pumping the booster amplifier in Fig. 7, and femtosecond main pulse broadening effect at some optical components into account, we can conclude that the contrast should be over 10^{10}, even though we use the booster amplifier with maximum pumping condition. We also plan to measure the pulse duration and contrast at full pumping energy for the booster amplifier. The background level is also expected to be the same as or less than the measured level in a nanosecond time scale [28,60]. Considering the extinction ratio, 62, of the ultrafast Pockels cell, the contrast is estimated to be close to 10^{12} on the nanosecond time scale. The energy outside the scanning range (650 ps) could be reduced considerably. The ASE background is generated mostly in the preamplifier stage. Our OPCPA preamplifier might generate several a nanoseconds pedestal with $\sim 10^{12}$ contrast; however, the energy outside this range should be much less. Therefore, we can expect that most of the energy is concentrated on our scanning range and that the analysis in this range would be interesting. We will also infer focused intensity capability on target by measuring the focused spot size of an attenuated pulse.

F. Improvements of Pointing Stability

We have installed and tested three automatic beam alignment systems at the front end of the laser system. The systems have been used for the pump lasers for the Ti:sapphire oscillator in the first CPA stage, for the OPCPA in the second CPA stage, and for the seed laser for the OPCPA after the first CPA stage. There are two main reasons for installation of the alignment system. The first is to bring the beams back to their set positions after switch-on of the laser system and, hence, to speed up the set-up procedure. The second is to compensate for thermal and mechanical drifts to keep the beam positions for minimizing the temporal variation in energy and pulse duration during laser operations. Beam positions of the seed laser for the OPCPA, for example, are monitored by two position-sensitive detectors (PSD) using leakage pulse energy through the back of two high-reflection mirrors (TEM Messtechnik GmbH, BeamLock). The PSD is an analog device that operates with a 10–100 μs response time, so it is fast enough to monitor short-term fluctuations attributed to causes such as air turbulence and vibrations of the optical elements and benches. The software controlling the system calculates the centroid positions. If a deviation from the predetermined set-point values is detected, the beam is steered back by means of motorized actuators fitted to mirror mounts located upstream from the PSDs. Motorized mirrors are preferred to piezo driven mirrors because they hold their position when powered off. T avoid the large fluctuations during stabilization due to the steep displacement, we introduce annalog circuit to carefully adjust a proportional-integral-derivative controller. We also modify the circuit to hold the peak value of the pulsed signal from the PSD sensor because the sensor does not generate a signal during the shot-to-shot time period to detect pulses beams. Figure 8 shows the beam positions after switch-on during a typical day. As can be seen from this figure, beams are initially displaced by some amount, corresponding to up to one beam diameter. After about 1 s, displacements are corrected. Actually, the stability of the whole system is perfect throughout the day. The result clearly demonstrates that the automatic alignment system has greatly improved the stability and consistency of the system's performance. We plan to extend this stabilization system throughout the J-KAREN laser chain.

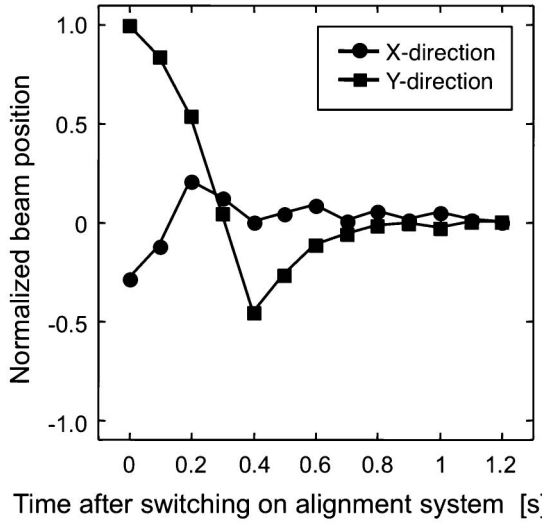

Fig. 8. Vertical and horizontal deviations of beam position after switch-on of the automatic beam alignment system.

3. Conclusion

We have successfully combined multiple techniques for realizing a high-spatiotemporal-quality petawatt-class Ti:sapphire laser system with the use of an OPCPA preamplifier in a double CPA and beam homogenization. The low-gain OPCPA preamplifier in the double-CPA scheme provides high temporal contrast, of over 10^{10}, on a subnanosecond time scale. The ultrafast Pockels cell yields a close to 10^{12} contrast on the nanosecond time scale. These results enable studies of ultrarelativistic laser–matter interaction at intensities of $10^{20}\mathrm{W/cm^2}$ or more. The capability of DOEs for beam homogenization to produce a uniform flat-topped energy distribution at the Ti:sapphire crystal has been demonstrated. A near-homogeneous amplified flat-top spatial intensity profile is obtained, minimizing the risk of damage in the large optical components. We have achieved the amplification of a broadband pulse greater than 30 J of uncompressed output energy, indicating the potential for reaching peak power in excess of 500 TW. Ultra-high-intensity, high-contrast, high-beam-quality optical pulses generated in our J-KAREN

laser represent a superior source for studying relativistic laser–matter interactions.

The authors acknowledge contributions by the Kansai Photon Science Institute staff at Japan Atomic Energy Agency and Central Laser Facility staff at Rutherford Appleton Laboratory for their support of this work. One of the authors, H. Kiriyama especially thanks N. Miyanaga, K. Sueda, T. Berthou, F. Reversat, S. Tisserand, and T. Müller-Wirts for stimulating discussions and encouragement. This work was supported by the Special Coordination Funds for Promoting Science and Technology (SCF) commissioned by the Ministry of Education, Culture, Sports, Science and Technology (MEXT) of Japan. This work was partly performed under the joint project between the Institute of Laser Engineering, Osaka University, and the Advanced Photon Research Center, Japan Atomic Energy Agency, on "Mono-energetic quantum beam science with PW lasers" commissioned by MEXT. This research was partially supported by a Ministry of Education, Science, Sports, and Culture of Japan (MESSC-JP) Grant-in-Aid for Scientific Research (A) 20244065, 2008. It was also partially supported by the "Consortium for Photon Science and Technology" program funded by the Special Coordination Funds for Promoting Science and Technology commissioned by MEXT of Japan.

References

1. D. Strickland and G. Mourou, "Compression of amplified chirped optical pulses," Opt. Commun. **56**, 219–221 (1985).
2. D. Umstadter, "Review of physics and applications of relativistic plasmas driven by ultra-intense lasers," Phys. Plasmas **8**, 1774–1785 (2001).
3. T. Ditmire, S. Bless, G. Dyer, A. Edens, W. Grigsby, G. Hays, K. Madison, A. Maltsev, J. Colvin, M. J. Edwards, R. W. Lee, P. Patel, D. Price, B. A. Remington, R. Sheppherd, A. Wootton, J. Zweiback, E. Liang, and K. A. Kielty, "Overview of future directions in high energy-density and high-field science using ultra-intense lasers," Radiat. Phys. Chem. **70**, 535–552 (2004).
4. M. Aoyama, K. Yamakawa, Y. Akahane, J. Ma, N. Inoue, H. Ueda, and H. Kiriyama, "0.85 PW, 33 fs Ti:sapphire laser," Opt. Lett. **28**, 1594–1596 (2003).
5. X. Liang, Y. Leng, C. Wang, C. Li, L. Lin, B. Zhao, Y. Jiang, X. Lu, M. Hu, C. Zhang, H. Lu, D. Yin, Y. Jiang, X. Lu, H. Wei, J. Zhu, R. Li, and Z. Xu, "Parasitic lasing suppression in high gain femtosecond petawatt Ti:sapphire amplifier," Opt. Express **15**, 15335–15341 (2007).
6. Z. Y. Wei, Z. H. Wang, P. Wang, W. J. Ling, J. F. Zhu, H. N. Han, and J. Zhang, "A compact 355 TW femtosecond Ti:sapphire laser facility and trend to high contrast ratio," J. Phys. Conf. Ser. **112**, 032003 (2008).
7. S. Fourmaux, S. Payeur, A. Alexandrov, S. Serbanescu, F. Martin, T. Ozaki, A. Kudryashov, and J. C. Kieffer, "Laser beam wavefront correction for ultra high intensities with the 200 TW laser system at the advanced laser light source," Opt. Express **16**, 11987–11994 (2008).
8. V. Yanovsky, V. Chvykov, G. Kalinchenko, P. Rousseau, T. Planchon, T. Matsuoka, A. Maksimchuk, J. Nees, G. Cheriaux, G. Mourou, and K. Krushelnick, "Ultra-high intensity-300 TW laser at 0.1 Hz repetition rate," Opt. Express **16**, 2109–2114 (2008).
9. C. J. Hoocker, J. L. Collier, O. Chekhlov, R. J. Clarke, E. J. Divall, K. Ertel, P. Foster, S. Hancock, S. J. Hawkes, P. Holligan, A. J. Langley, W. J. Lester, D. Neely, B. T. Parry, and B. E. Wyborn, "The Astra Gemini petawatt Ti:sapphire laser," Rev. Laser Eng. **37**, 443–448 (2009).
10. S.-W. Bahk, P. Rousseau, T. A. Planchon, V. Chvykov, G. Kalintchenko, A. Maksimchuk, G. A. Mourou, and V. Yanovsky, "Generation and characterization of the highest laser intensities (10^{22}W/cm^2)," Opt. Lett. **29**, 2837–2839 (2004).
11. T. Ceccotti, A. Lévy, H. Popescu, F. Réau, P. D'Oliveira, P. Monot, J. P. Geindre, E. Lefebvre, and P. Martin, "Proton acceleration with high-intensity ultrahigh-contrast laser pulses," Phys. Rev. Lett. **99**, 185002 (2007).
12. P. Antici, J. Fuchs, E. d'Humières, E. Lefebvre, M. Borghesi, E. Brambrink, C. A. Cecchetti, S. Gaillard, L. Romagnani, Y. Sentoku, T. Toncian, O. Willi, P. Audebert, and H. Pépin, "Energetic protons generated by ultrahigh contrast laser pulses interacting with ultrathin targets," Phys. Plasmas **14**, 030701 (2007).
13. E. Esarey, C. B. Schroeder, and W. P. Leemans, "Physics of laser-driven plasma-based electron accelerators," Rev. Mod. Phys. **81**, 1229–1286 (2009).
14. Y. Fukuda, A. Ya. Faenov, M. Tampo, T. A. Pikuz, T. Nakamura, M. Kando, Y. Hayashi, A. Yogo, H. Sakaki, T. Kameshima, A. S. Pirozhkov, K. Ogura, M. Mori, T. Zh. Esirkepov, J. Koga, A. S. Boldarev, V. A. Gasilov, A. I. Magunov, T. Yamauchi, R. Kodama, P. R. Bolton, Y. Kato, T. Tajima, H. Daido, and S. V. Bulanov, "Energy increase in multi-MeV ion acceleration in the interaction of a short pulse laser with a cluster-gas target," Phys. Rev. Lett. **103**, 165002 (2009).
15. A. Rousse, K. T. Phuoc, R. Shah, A. Pukhov, E. Lefebvre, V. Malka, S. Kiselev, F. Burgy, J.-P. Rousseau, D. Umstadter, and D. Hulin, "Production of a keV x-ray bean from synchrotron radiation in relativistic laser-plasma interaction," Phys. Rev. Lett. **93**, 135005 (2004).
16. M. Kando, Y. Fukuda, A. S. Pirozhkov, J. Ma, I. Daito, L.-M. Chen, T. Zh. Esirkepov, K. Ogura, T. Homma, Y. Hayashi, H. Kotaki, A. Sagisaka, M. Mori, J. K. Koga, H. Daido, S. V. Bulanov, T. Kimura, Y. Kato, and T. Tajima, "Demonstration of laser-frequency upshift by electron-density modulations in a plasma wakefield," Phys. Rev. Lett. **99**, 135001 (2007).
17. Y. Fukuda, A. Ya. Faenov, T. Pikuz, M. Kando, H. Kotaki, I. Daito, J. Ma, L. M. Chen, T. Homma, K. Kawase, T. Kameshima, T. Kawachi, H. Daido, T. Kimura, T. Tajima, Y. Kato, and S. V. Bulanov, "Soft x-ray source for nanostructure imaging using femtosecond-laser-irradiated clusters," Appl. Phys. Lett. **92**, 121110 (2008).
18. K. Ogura, T. Shizuma, T. Hayakawa, A. Yogo, M. Nishiuchi, S. Orimo, A. Sagisaka, A. Pirozhkov, M. Mori, H. Kiriyama, S. Kanazawa, S. Kondo, Y. Nakai, T. Shimoura, M. Tanoue, A. Akutsu, T. Motomura, H. Okada, T. Kimura, Y. Oishi, T. Nayuki, T. Fujii, K. Nemoto, and H. Daido, "Proton-induced nuclear reactions using compact high-contrast high-intensity laser," Appl. Phys. Exp. **2**, 066001 (2009).
19. B. Dromey, M. Zepf, A. Gopal, K. Lancaster, M. S. Wei, K. Krusheknick, M. Tatarakis, N. Vakakis, S. Moustaizis, R. Kodama, M. Tanpo, C. Stoeckl, R. Clarke, H. Habara, D. Neely, S. Karsch, and P. Norreys, "High harmonic generation in the relativistic limit," Nature Phys. **2**, 456–459 (2006).
20. D. Neely, P. Foster, A. Robinson, F. Lindau, O. Lundh, A. Persson, C. G. Wahlström, and P. McKenna, "Enhanced proton beams from ultrathin targets driven by high contrast laser pulse," Appl. Phys. Lett. **89**, 021502 (2006).
21. J. Itatani, J. Faure, M. Nantel, G. Mourou, and S. Watanabe, "Suppression of the amplified spontaneous emission in chirped-pulse-amplification lasers by clean high-energy seed-pulse injection," Opt. Commun. **148**, 70–74 (1998).
22. H. Kiriyama, M. Mori, Y. Nakai, T. Shimomura, M. Tanoue, A. Akutsu, H. Okada, T. Motomura, S. Kondo, S. Kanazawa, A. Sagisaka, J. Ma, I. Daito, H. Kotaki, H. Daido, S. Bulanov,

T. Kimura, and T. Tajima, "Generation of high-contrast and high-intensity laser pulses using an OPCPA preamplifier in a double CPA, Ti:sapphire laser system," Opt. Commun. **282**, 625–628 (2009).
23. A. Renault, F. A. Rochereau, T. Planchon, P. D. Oliveira, T. Auguste, G. Chériaux, and J. P. Chambaret, "ASE contrast improvement with a non-linear filtering Sagnac interferometer," Opt. Commun. **248**, 535–541 (2005).
24. M. P. Kalashnikov, E. Risse, H. Schönnagel, and W. Sandner, "Double chirped-pulse-amplification laser: a way to clean pulses temporally," Opt. Lett. **30**, 923–925 (2005).
25. N. Minkovski, G. I. Petrov, S. M. Saltiel, O. Albert, and J. Etchepare, "Nonlinear polarization rotation and orthogonal polarization generation experienced in a single-beam configuration," J. Opt. Soc. Am. B **21**, 1659–1664 (2004).
26. A. Jullien, O. Albert, F. Burgy, G. Hamoniaux, J. P. Rousseau, J. P. Chambaret, F. Augé-Rochereau, G. Chériaux, J. Etchepare, N. Minkovski, and S. M. Saltiel, "10^{-10} temporal contrast for femtosecond ultraintense lasers by cross-polarized wave generation," Opt. Lett. **30**, 920–922 (2005).
27. G. Doumy, F. Quéré, O. Gobert, M. Perdrix, Ph. Martin, P. Audebert, J. C. Gauthier, J. P. Geindre, and T. Wittmann, "Complete characterization of a plasma mirror for the production of high-contrast ultraintense laser pulses," Phys. Rev. E **69**, 026402 (2004).
28. C. Thaur, F. Quéré, J.-P. Geindre, A. Levy, T. Ceccotti, P. Monot, M. Bougeard, F. Réau, P. D'okiveira, P. Audebert, R. Marjoribanks, and P. H. Martin, "Plasma mirrors for ultrahigh-intensity optics," Nature Phys. **3**, 424–429 (2007).
29. V. Chvykov, P. Rousseau, S. Reed, G. Kalinchenko, and V. Yanovsky, "Generation of 10^{11} contrast 50 TW laser pulses," Opt. Lett. **31**, 1456–1458 (2006).
30. L. Antonucci, J. P. Rousseau, A. Jullien, B. Mercier, V. Laude, and G. Cheriaux, "14 fs high temporal quality injector for ultra-high intensity laser," Opt. Commun. **282**, 1374–1379 (2009).
31. A. Dubietis, G. Jonusauskas, and A. Piskarskas, "Powerful femtosecond pulse generation by chirped and stretched pulse parametric amplification in BBO crystal," Opt. Commun. **88**, 437–440 (1992).
32. I. N. Ross, P. Matousek, M. Towrie, A. J. Langley, and J. L. Collier, "The prospects for ultrashort pulse duration and ultrahigh intensity using optical parametric chirped pulse amplifiers," Opt. Commun. **144**, 125–133 (1997).
33. Y. Kitagawa, H. Fujita, R. Kodama, H. Yoshida, S. Matsuo, T. Jitsuno, T. Kawasaki, H. Kitamura, T. Kanabe, S. Sakabe, K. Shigemori, N. Miyanaga, and Y. Izawa, "Prepulse-free petawatt laser for a fast ignitor," IEEE J. Quantum Electron. **40**, 281–293 (2004).
34. I. O. Musgrave, C. Hernandez-Gomez, D. Canny, J. Collier, and R. Heathcote, "Minimization of the impact of a broad bandwidth high-gain nonlinear preamplifier to the amplified spontaneous emission pedestal of the Vulcan petawatt laser facility," Appl. Opt. **46**, 6978–6983 (2007).
35. N. Blanchot, G. Behar, T. Berthier, E. Bignon, F. Boubault, C. Chappuis, H. Coïc, C. Damiens-Dupont, J. Ebrardt, Y. Gautheron, P. Gibert, O. Hartmann, E. Hugonnot, F. Laborde, D. Lebeaux, J. Luce, S. Montant, S. Noailles, J. N´eauport, D. Raffestin, B. Remy, A. Roques, F. Sautarel, M. Sautet, C. Sauteret, and C. Rouyer, "Overview of PETAL, multi-petawatt project on the LIL facility," Plasma Phys. Controlled Fusion **50**, 124045 (2008).
36. J. Schwarz, P. Rambo, M. Geissel, M. Kimmel, E. Brambrink, B. Atherton, and J. Glassman, "A hybrid OPCPA/Nd: phosphate glass multi-terawatt laser system for seeding of a petawatt laser," Opt. Commun. **281**, 4984–4992 (2008).
37. F. Ple, M. Pittman, G. Jamelot, and J. P. Chambaret, "Design and demonstration of a high-energy booster amplifier for a high-repetition rate petawatt class laser system," Opt. Lett. **32**, 238–240 (2007).
38. K. Ertel, C. Hooker, S. J. Hawkes, B. T. Parry, and J. L. Collier, "ASE suppression in a high energy titanium sapphire amplifier," Opt. Express **16**, 8039–8049 (2008).
39. G. Cheriaux, P. Rousseau, F. Salin, J. P. Chambaret, B. Walker, and L. F. Dimauro, "Aberration-free stretcher design for ultrashort-pulse amplification," Opt. Lett. **21**, 414–416 (1996).
40. F. Tavella, A. Marcinkevicius, and F. Krausz, "Investigation of the superfluorescence and signal amplification in an ultrabroadband multiterawatt optical parametric chirped pulse amplifier system," New J. Phys. **8**, 219 (2006).
41. H. Okada, H. Kiriyama, M. Mori, Y. Nakai, T. Shimomura, M. Tanoue, S. Kondo, S. Kanazawa, H. Daido, T. Kimura, and T. Tajima, "Demonstration of highly efficient broadband amplification in an optical parametric chirped-pulse amplifier system," Opt. Rev. **16**, 1–3 (2009).
42. R. C. Shah, R. P. Johnson, T. Shimada, K. A. Flippo, J. C. Fernandez, and B. M. Hegelich, "High-temporal contrast using low-gain optical parametric amplification," Opt. Lett. **34**, 2273–2275 (2009).
43. H. Kiriyama, M. Mori, Y. Nakai, Y. Yamamoto, M. Tanoue, A. Akutsu, T. Shimomura, S. Kondo, S. Kanazawa, H. Daido, T. Kimura, and N. Miyanaga, "High-energy, high-contrast, multiterawatt laser pulses by optical parametric chirped-pulse amplification," Opt. Lett. **32**, 2315–2317 (2007).
44. V. Bagnoud, I. A. Begishev, M. J. Guardalben, J. Puth, and J. D. Zuegel, "5 Hz, >250 mJ optical parametric chirped-pulse amplifier at 1053 nm," Opt. Lett. **30**, 1843–1845 (2005).
45. P. Wnuk, Y. Stepanenko, and C. Radzewicz, "Multi-terawatt chirped pulse optical parametric amplifier with a time-shear power amplification stage," Opt. Express **17**, 15264–15273 (2009).
46. O. V. Chekhlov, J. L. Collier, I. N. Ross, P. K. Bates, M. Notley, C. Hernandez-Gomez, W. Shaikh, C. N. Danson, D. Neely, P. Matousek, and S. Hancock, "35 J broadband femtosecond optical parametric chirped pulse amplification system," Opt. Lett. **31**, 3665–3667 (2006).
47. M. Suzuki, H. Kiriyama, I. Daito, H. Okada, Y. Nakai, S. Orimo, M. Sato, Y. Tamaoki, T. Yoshii, J. Maeda, S. Matsuoka, H. Kan, P. R. Bolton, H. Daido, and S. Kawanishi, "Multi-millijoule, nonlinear preamplifier for high intensity femtosecond Yb:YAG chirped-pulse amplification lasers at 1030 nm," Appl. Phys. B **97**, 379–382 (2009).
48. H. Kiriyama, N. Inoue, Y. Akahane, and K. Yamakawa, "Prepulse-free, multi-terawatt, sub-30 fs laser system," Opt. Express **14**, 438–445 (2006).
49. M. Pittman, S. Ferré, J. P. Rousseau, L. Notebaert, J. P. Chambaret, and G. Chériaux, "Design and characterization of a near-diffraction-limited femtosecond 100 TW 10 Hz high-intensity laser system," Appl. Phys. B **74**, 529–535 (2002).
50. H. Kiriyama, M. Mori, Y. Nakai, T. Shimomura, M. Tanoue, A. Akutsu, S. Kondo, S. Kanazawa, H. Okada, T. Motomura, H. Daido, T. Kimura, and T. Tajima, "High-contrast, high-intensity laser pulse generation using a nonlinear preamplifier in a Ti:sapphire laser system," Opt. Lett. **33**, 645–647 (2008).
51. T. A. Planchon, W. Amir, C. Childress, J. A. Squier, and C. G. Durfee, "Measurement of pump-induced transient lensing in a cryogenically-cooled high average power Ti:sapphire amplifier," Opt. Express **16**, 18557–18564 (2008).
52. D. Eimerl, "Quadrature frequency conversion," IEEE J. Quantum Electron. **23**, 1361–1371 (1987).
53. H. Kiriyama, F. Nakano, and K. Yamakawa, "High-efficiency frequency doubling of a Nd:YAG laser in a two-pass quadrature frequency-conversion scheme using $CsLiB_6O_{10}$ crystals," J. Opt. Soc. Am. B **19**, 1857–1864 (2002).

54. M. Tanaka, H. Kiriyama, Y. Ochi, Y. Nakai, H. Sasao, H. Okada, H. Daido, P. Bolton, and S. Kawanishi, "High-energy, spatially flat-top green pump laser by beam homogenization for petawatt scale Ti:sapphire laser systems," Opt. Commun. **282**, 4401–4403 (2009).
55. H. Kiriyama, M. Tanaka, Y. Ochi, Y. Nakai, H. Sasao, H. Okada, M. Mori, T. Shimomura, S. Kanazawa, H. Daido, P. Bolton, and S. Kawanishi, "100 J level green laser beam homogenization to pump a petawatt class Ti:sapphire chirped-pulse amplification laser system," Rev. Laser Eng. **37**, 467–469 (2009).
56. F. G. Patterson, J. Bonlie, D. Price, and B. White, "Suppression of parasitic lasing in large-aperture Ti:sapphire laser amplifiers," Opt. Lett. **24**, 963–965 (1999).
57. N. Forget, A. Cotel, E. Brambrink, P. Audebert, C. L. Blanc, A. Jullien, O. Albert, and G. Chériaux, "Pump-noise transfer in optical parametric chirped-pulse amplification," Opt. Lett. **30**, 2921–2923 (2005).
58. V. Bagnoud, J. D. Zuegel, N. Forget, and C. Le Blanc, "High-dynamic-range temporal measurements of short pulses amplified by OPCPA," Opt. Express **15**, 5504–5511 (2007).
59. L. M. Frantz and J. S. Nodvik, "Theory of pulse propagation in a laser amplifier," J. Appl. Phys. **34**, 2346–2349 (1963).
60. K.-H. Hong, B. Hou, J. A. Nees, E. Power, and G. A. Mourou, "Generation and measurement of $>10^8$ intensity contrast ratio in a relativistic kHz chirped-pulse amplified laser," Appl. Phys. B **81**, 447–457 (2005).